GeroScience (2024) 46:6395–6417
https://doi.org/10.1007/s11357-024-01264-3

ORIGINAL ARTICLE

Proteomic analysis of lung responses to SARS-CoV-2 infection in aged non-human primates: clinical and research relevance

Andreu Garcia-Vilanova · Anna Allué-Guardia · Nadine M. Chacon · Anwari Akhter · Dhiraj Kumar Singh · Deepak Kaushal · Blanca I. Restrepo · Larry S. Schlesinger · Joanne Turner · Susan T. Weintraub · Jordi B. Torrelles

Received: 19 March 2024 / Accepted: 21 June 2024 / Published online: 6 July 2024

Abstract With devastating health and socioeconomic impact worldwide, much work is left to understand the Coronavirus Disease 2019 (COVID-19), with emphasis in the severely affected elderly population. Here, we present a proteomics study of lung tissue obtained from aged *vs.* young rhesus macaques (*Macaca mulatta*) and olive baboons (*Papio Anubis*) infected with severe acute respiratory syndrome coronavirus 2 (SARS-CoV-2). Using age as a variable, we identified common proteomic profiles in the lungs of aged infected non-human primates (NHPs), including key regulators of immune function, as well as cell and tissue remodeling, and discuss the potential clinical relevance of such parameters. Further, we identified key differences in proteomic profiles between both NHP species, and compared those to what is known about SARS-CoV-2 in humans. Finally, we explored the translatability of these animal models in the context of aging and the human presentation of the COVID-19.

Keywords Aging · SARS-CoV-2 · COVID-19 · Lung proteomics · Non-human primates

Supplementary Information The online version contains supplementary material available at https://doi.org/10.1007/s11357-024-01264-3.

A. Garcia-Vilanova (✉) · A. Allué-Guardia (✉) · N. M. Chacon · A. Akhter · D. K. Singh · D. Kaushal · L. S. Schlesinger · J. Turner · J. B. Torrelles (✉)
Population Health, Host Pathogen Interactions, and Disease Prevention and Intervention Programs, Texas Biomedical Research Institute, San Antonio, TX, USA
e-mail: garciavilanovaandreu@gmail.com

A. Allué-Guardia
e-mail: aallueguardia@txbiomed.org

J. B. Torrelles
e-mail: jtorrelles@txbiomed.org

A. Allué-Guardia · B. I. Restrepo · L. S. Schlesinger · J. Turner · J. B. Torrelles
International Center for the Advancement of Research & Education (I•CARE), Texas Biomedical Research Institute, San Antonio, TX, USA

N. M. Chacon
Integrated Biomedical Sciences Program, University of Texas Health Science Center at San Antonio, San Antonio, TX, USA

B. I. Restrepo
University of Texas Health Science Center at Houston, School of Public Health, Brownsville Campus, Brownsville, TX, USA

B. I. Restrepo
South Texas Diabetes and Obesity Institute, University of Texas Rio Grande Valley, Edinburg, TX, USA

Present Address:
J. Turner
Abigail Wexner Research Institute at Nationwide Children's Hospital, Columbus, OH, USA

Introduction

With an estimated 774 million cases or more reported and 0.90% mortality globally [1], the Coronavirus disease (COVID-19) pandemic is still an unresolved public health concern. Aged individuals, and especially, those with pre-existing co-morbidities, are at increased risk of respiratory complications and even death [2, 3]. Indeed, a 62-fold increase in mortality after severe acute respiratory syndrome coronavirus 2 (SARS-CoV-2) infection has been reported in the > 65-year-old age group compared to the < 55 age group [4, 5].

Despite abundant research to understand COVID-19 pathogenesis, we still lack information on specific tissue responses driven by the infection. Most published proteomic reports are from human clinical samples obtained *post-mortem* [6–8], with limited, if any, studies investigating key differences in lung-specific responses related to the age of the individuals.

To address this knowledge gap, here we used pre-existing lung samples from our established models of severe acute respiratory syndrome coronavirus 2 (SARS-CoV-2) infection in non-human primates (NHPs) [9–12]. We sought to identify differences in the proteomes of two age groups (aged *vs.* young) in two NHP species, rhesus macaques (*Macaca mulatta*) and olive baboons (*Papio anubis*) during SARS-CoV-2 infection. We previously published that both species are susceptible to SARS-CoV-2, with baboons having more lung inflammation and longer SARS-CoV-2 viral shedding compared to macaques [9]. Their differential progression to COVID-19 makes them suitable as models to test vaccines and therapies. Global proteomics were conducted to obtain their proteomic profiles and relative quantification in the lungs at the time of necropsy (14 days post-infection), and results were then compared to published reports from human infections.

S. T. Weintraub
Department of Biochemistry and Structural Biology, University of Texas Health Science Center at San Antonio, San Antonio, TX, USA

Materials and methods

Study approval Pre-existing samples used in this study were from infected NHPs that were housed under Animal Biosafety Level 3 (ABSL3) facilities at the Southwest National Primate Research Center (SNPRC), where they were treated according to the standards recommended by AAALAC International and the NIH Guide for the Care and Use of Laboratory Animals. NHP studies were approved by the Institutional Animal Care and Use Committee (IACUC) at Texas Biomedical Research Institute (protocol# 1714 PC 6).

Animal study and tissue processing We used a biorepository of pre-existing lung tissue samples from 3-year-old (young group, $n = 6$) and 17 to 22-year-old (aged group, $n = 8$) rhesus macaques and 2-year-old (young group, $n = 6$) and 10 to 20-year-old (aged group, $n = 7$) olive baboons; gender matched, infected with SARS-CoV-2 USA/WA1 2020 strain through multiple routes (ocular, intratracheal and intranasal) with a dose of 1.05×10^6 PFU/per animal. Lung tissues were collected at necropsy after 14 days post-infection as described [9]. Briefly, approximately 0.5 cm^3 tissues pieces were obtained at necropsy and snap-frozen with dry ice and stored at -80 °C until processing. Tissues were thawed in ice and homogenized in a total of 2 mL of 1X DPBS containing 1% SDS and a protease inhibitor cocktail (Roche) using Precellys Lysing Kit (CKMix50 – 7 mL). After homogenization, samples were filtered to remove large debris, and were inactivated at 60 °C for 1 h [9].

Proteomic analyses Lung homogenate samples were mixed with 10% SDS/50 mM triethyl-ammonium bicarbonate (TEAB) in the presence of protease and phosphatase inhibitors (Halt; Thermo Scientific). Aliquots corresponding to 100 µg protein (EZQ™ Protein Quantitation Kit; Thermo Fisher) were reduced with tris(2-carboxyethyl)phosphine hydrochloride (TCEP), alkylated in the dark with iodoacetamide and applied to S-Traps (mini; Protifi) for tryptic digestion (sequencing grade; Promega) in 50 mM TEAB. Peptides were eluted from the S-Traps with 0.2% formic acid in 50% aqueous acetonitrile and quantified using Pierce™ Quantitative Fluorometric Peptide Assay (Thermo Scientific).

DIA-MS (Data Independent Acquisition Mass Spectrometry) was conducted on an Orbitrap Fusion Lumos (Thermo Scientific) mass spectrometer. Online HPLC separation used an RSLC NANO HPLC system (Thermo Scientific/Dionex: column, PicoFrit™ (New Objective; 75 µm i.d.) packed to 15 cm with C18 adsorbent (Vydac; 218MS 5 µm, 300 Å); mobile phase A, 0.5% acetic acid (HAc)/0.005% trifluoroacetic acid (TFA) in water; mobile phase B, 90% acetonitrile/0.5% HAc/0.005% TFA/9.5% water; gradient 3 to 42% B in 120 min; flow rate, 0.4 µl/min. A pool was made of all of the samples, and 2-µg peptide aliquots were analyzed using gas-phase fractionation and 4-m/z windows (30 k resolution for precursor and product ion scans, all in the orbitrap) to create a DIA chromatogram library [13] by searching against a Prosit-generated predicted spectral library (Gessulat 2019) [14] based on either the reference protein sequence database for UniProt_Papio_anubis_9555_20220312 (44,734 sequences; 24,127,678 residues) or UniProt_Macaca_mulatta_9544_20220315 (44,390 sequences; 28,513,169 residues), as appropriate for the experiment. A database of common contaminants (without any bovine serum protein entries; 124 sequences; 62,564 residues) was also used. Experimental samples were randomized for sample preparation and analysis. Injections of 2 µg of peptides were employed. MS data for experimental samples were acquired in the Orbitrap using 8-*m/z* windows (staggered; 30 k resolution for precursor and product ion scans) and searched against the chromatogram library. Carbamidomethylation of cysteine was considered as a fixed modification for generation of the chromatogram library and for searching the MS data from the experimental samples. Scaffold DIA (v3.2.1; Proteome Software) was used for all DIA-MS data processing.

Data and statistical analyses Protein identifiers were transformed to gene symbols by: 1- Annotated gene name, 2- Sequence homology. Significant DAPs were selected based on the following thresholds: Log_2 Fold Change < -0.5 or > 0.5, *p*-value < 0.05. IPA (v90348151; QIAGEN) was used to perform pathway analysis, pathway comparison between species, and regulator prediction analyses. R v4.2.2 was used to generate Volcano plots (EnhancedVolcano package), with supporting packages Bioconductor and ggplot2. Heatmaps were generated in NG-CHM Heat Map Viewer v2.22.2 [15, 16].

Results and discussion

Comparative proteomics of SARS-CoV-2 infected lung tissues from aged vs. young rhesus macaques and olive baboons – shared DAPs

We performed untargeted proteomics by DIA-MS in pre-existing samples of lung tissue of SARS-CoV-2 infected rhesus macaques and olive baboons [9] for the identification and relative quantification of proteins in infected NHPs. We first determined significant Differentially Abundant Proteins (DAPs) (log_2 fold change ≤ -0.5 or ≥ 0.5, *p*-value < 0.05) in both aged *vs.* young rhesus macaques (RM) and olive baboons (OB), with rhesus macaques having 120 and olive baboons 203 total DAPs (Fig. 1, Tables 1 and 2). Of those, 11 DAPs were shared between both species, and 109 and 192 DAPs were exclusive to rhesus and baboons, respectively (Fig. 1A).

Of the 11 shared DAPs, three were significantly upregulated in both NHP species when comparing aged *vs.* young animals (Fig. 1A, Tables 1 and 2) (listed here as human protein, followed by gene name equivalent and log_2 fold changes in both NHPs). Serum amyloid P-component or SAP [APCS (RM 1.14/OB 2.99)] is a pentraxin associated with amyloid deposits with roles in innate and acute immune responses. Increased SAP levels could potentially be linked to disease severity since other serum amyloid-associated proteins (e.g. Serum amyloid A-component) are known markers of COVID-19 severity [17, 18]. This was followed by the upregulation of Immunoglobulin heavy constant mu [IGHM (RM 1.06/OB 1.35)] and Immunoglobulin J chain [JCHAIN (RM 0.73/OB 1.78)], both components of immunoglobulin M (IgM), directly associated with SARS-CoV-2 infection and regulation of the host complement system. High IgM levels have been associated with an altered immune response and represent a risk factor for the development of recurrent lung infections, such as SARS-CoV-2 [19].

The remaining eight DAPs were significantly downregulated in both NHP species (aged *vs.* young) during early stages of SARS-CoV-2 infection (Fig. 1A, Tables 1 and 2): Host cell factor 1

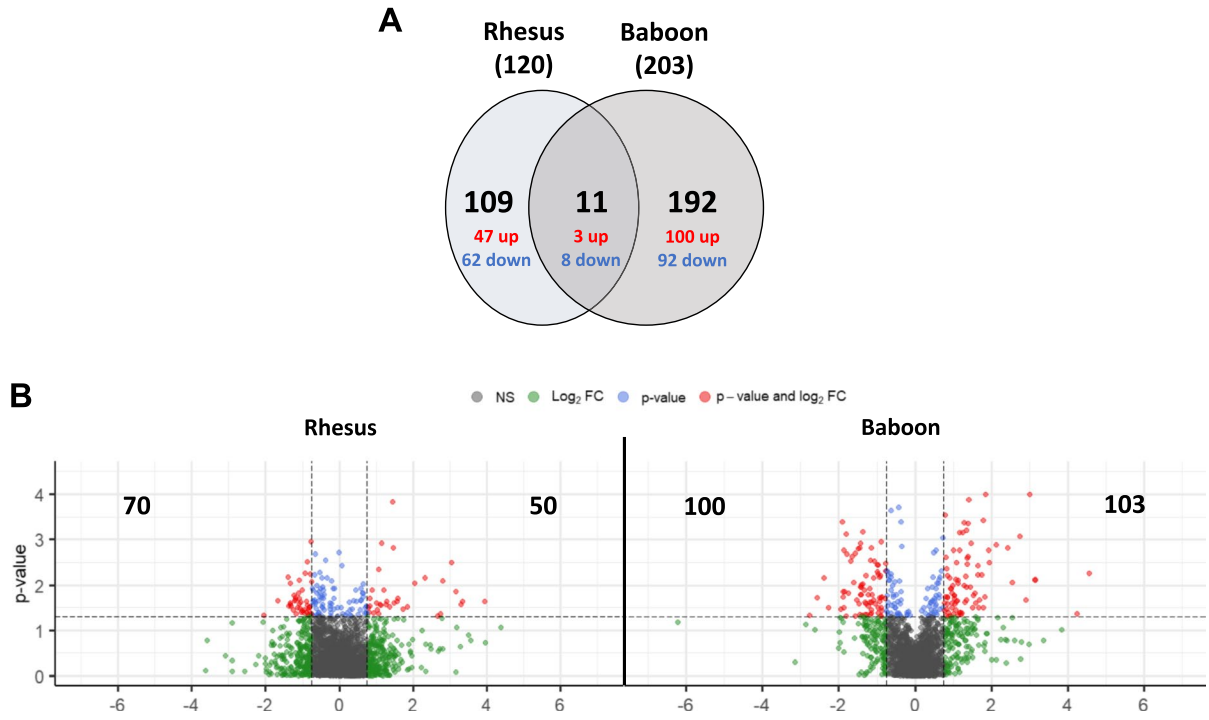

Fig. 1 Differentially expressed proteins (DAPs) in aged *vs.* young rhesus macaques and aged *vs.* young olive baboons. **A** Venn diagram showing the number of shared and unique DAPs in each NHP species; **B** Volcano plots showing the distribution of DAPs. The x-axis shows $\log_2$-transformed protein fold changes, the y-axis shows $-\log_{10}$-transformed *p*-values; a total of 120 DAPs and 203 DAPs were identified for aged rhesus macaque and olive baboon groups, respectively

[HCFC1 (RM -1.04/OB -0.707)] is crucial to regulate the host cell cycle and is recognized by SARS-CoV-2 [20], although no direct correlation with COVID-19 progression has been described. Liprin-alpha-1 [PPFIA1 (RM -1.02 /OB -0.696)], a LAR family transmembrane protein-tyrosine phosphatase involved in cell–matrix interactions [21], was previously identified as a potential gene candidate of Acute Lung Injury (ALI) risk [22], which is the most severe form of COVID-19, and has also been linked to age-associated changes [23]. Next is far upstream element-binding protein 2 [KHSRP or FUBP2 (RM -0.814/OB -0.719)], involved in mRNA biogenesis, stability and trafficking, and regulation of innate and adaptive immune responses, with decreased host antiviral defense in their absence [24, 25], which could be associated with the increased disease pathology and susceptibility observed in aged animals. Further, we observed downregulation of transcription elongation factor SPT5 [SUPT5H (RMs -0.651/OB -1.23)], a component of the DRB sensitivity-induced complex (DSIF) that regulates mRNA processing and facilitates rapid induction of pro-inflammatory genes through NF-κB activation [26, 27]. SPT5 downregulation would result in decreased immune response, which could favor SARS-CoV-2 replication.

Two RNA-binding proteins (RBPs) were also downregulated in both NHP species. RBP Raly [RALY (RM -0.533/OB -0.892)] targets ssRNAs and acts as an antiviral, although the SARS-CoV-2 genome was found to be depleted of interacting motifs with RALY, suggesting that the viral genome might have evolved to avoid interactions with this host defense protein [28]. Still, this might be a double-edged sword, with viral evasion and lower basal levels to respond against infection. On the other hand, RBP RO60 [RO60 (RM -0.605/OB -0.627)] binds to non-coding misfolded Y RNAs, and regulates some pro-inflammatory genes in autoimmune disorders such as Guillain-Barré syndrome and rheumatoid arthritis. Autoantibodies against RO60 are found in COVID-19 patients, suggestive of some viral-host interaction [29].

Table 1 List of DAPs for rhesus macaques (aged *vs.* young). Accession number, protein name, gene name, *p*-value and $\log_2$ Fold Change are provided. Proteins are ordered by increasing *p*-value. Top 5 DAPs are highlighted in bold

Accession Number	Protein name	Gene name	*p*-value	Log2 Aged Rhesus
F7EDT3	**Calpain 5**	**CAPN5**	**0.00015**	**1.45**
F6TSU2	**Protein-tyrosine-phosphatase receptor J**	**PTPRJ**	**0.0011**	**-0.771**
F7H1V9	**Pentraxin**	**APCS**	**0.0012**	**1.14**
F6UQB6	**Heme-binding protein 1**	**HEBP1**	**0.0015**	**1.46**
F6V089	**t-SNARE coiled-coil homology domain-containing protein**	**PPP1R8**	**0.0021**	**-0.644**
A0A1D5Q9N1	Radixin	RDX	0.0031	-0.875
F7ESZ3	Biglycan	BGN	0.0032	3.03
A0A1D5R6M8	Immunoglobulin heavy constant mu	IGHM	0.0045	1.06
A0A5F7ZIS1	RALY heterogeneous nuclear ribonucleoprotein	RALY	0.0052	-0.533
F6YXJ2	Deoxyribonuclease II	DNASE2	0.0054	-0.936
F6R2V4	BAG cochaperone 3	BAG3	0.0057	-0.799
F7C9U4	CD93 molecule	CD93	0.0059	-0.669
H9FSW2	Argonaute RISC component 1	AGO1	0.0066	-1.38
F6RJC0	1-phosphatidylinositol 4,5-bisphosphate phosphodiesterase	PLCB3	0.007	2.33
F6SFP9	D-aminoacyl-tRNA deacylase	DTD1	0.0079	-1.1
A0A1D5QRS2	Histone H2A	H2AC12	0.0082	2.81
F6ZAW8	Hippocalcin like 1	HPCAL1	0.0085	-0.755
G7MHG1	Complement C1q subcomponent subunit B	C1QB	0.0089	2.05
F7GPV6	Multifunctional protein ADE2	PAICS	0.0092	-1.34
A0A5F7ZHW5	Lectin, mannose binding 2	LMAN2	0.0095	0.64
F7FMM5	TROVE domain-containing protein	RO60	0.01	-0.605
A0A5F7ZQM9	Proteasome 20S subunit beta 8	PSMB8	0.012	-0.726
A0A1D5Q716	Uncharacterized protein	MCAM	0.012	-0.519
A0A5F7Z998	Vitronectin	VTN	0.012	0.589
A0A1D5Q3K1	NAD(P)H-hydrate epimerase	NAXE	0.013	-1.02
F7EHH7	Protein-tyrosine-phosphatase	PTPRG	0.013	-0.71
A0A5F8A5N3	Uncharacterized protein	NAPG	0.013	0.893
F7E8L2	Phosphoenolpyruvate carboxykinase (GTP)	PCK2	0.013	1.21
P00002	Cytochrome c	CYCS	0.014	-0.56
F7HSJ5	Histone H2A	H2AC21	0.014	3.15
A0A5F7ZEM7	Early endosome antigen 1	EEA1	0.015	-1.11
A0A1D5QTI7	60S ribosomal protein L17	RPL17	0.015	-0.605
F7DJM1	SEC22 vesicle-trafficking protein homolog B	SEC22B	0.015	0.62
F6UZQ6	Reticulon	RTN4	0.015	0.637
F7H9U1	Latent transforming growth factor beta binding protein 4	LTBP4	0.017	-1.24
G7N7C5	Citrate synthase	CS	0.018	-0.523
A0A1D5Q3X0	Cysteinyl-tRNA synthetase	CARS1	0.018	0.642
A0A1D5R2U5	IK cytokine	IK	0.019	-1.2
A0A1D5RGB7	EWS RNA binding protein 1	EWSR1	0.02	-1.1
F6YK65	C3/C5 convertase	CFB	0.02	0.827
F6QAX2	Tubulin beta chain	TUBB3	0.02	1.58
F6W1K5	UBX domain protein 1	UBXN1	0.021	-1.2
A0A5F7ZJ61	Transforming acidic coiled coil containing protein 2	TACC2	0.021	-0.671

Table 1 (continued)

Accession Number	Protein name	Gene name	*p*-value	Log2 Aged Rhesus
A0A5F7ZWV4	Secernin 1	SCRN1	0.021	0.576
A0A1D5RGN2	Cell adhesion molecule 1	CADM1	0.022	-1.66
A0A1D5Q4R1	Protein-tyrosine-phosphatase	PTPRM	0.022	-1.22
A0A1D5R9J9	Nucleoside diphosphate kinase	NME3	0.022	-0.721
F7CA88	Ribonuclease inhibitor	LOC720791	0.022	-0.558
A0A5F7Z9N3	60S ribosomal protein L4	RPL4	0.022	0.587
F7H400	Kinectin 1	KTN1	0.023	-0.898
A0A5F8APU1	U6 snRNA-associated Sm-like protein LSm4	LSM4	0.023	-0.697
A0A5F7ZVB9	Inter-alpha-trypsin inhibitor heavy chain 2	ITIH2	0.023	1.28
F6UZ20	Fibrinogen gamma chain	FGG	0.023	1.57
A0A1D5R0R7	Histone H2B	H2BC5	0.023	3.33
F7HAP4	Histone H2A	H2AC6	0.023	3.94
F7CDG7	U1 small nuclear ribonucleoprotein 70 kDa	SNRNP70	0.024	-1.05
A0A1D5RJP5	Arylsulfatase B	ARSB	0.024	-0.66
F6TCB7	Bis(5'-adenosyl)-triphosphatase	FHIT	0.025	-1.33
A0A5F7ZHK9	H15 domain-containing protein	H1-2	0.025	1.01
F6QXG0	Angiopoietin-2	ANGPT2	0.025	1.49
A0A5F7ZA28	Uncharacterized protein	FUBP3	0.026	-1.1
A0A5F7ZC04	Transcription elongation factor SPT5	SUPT5H	0.026	-0.651
A0A1D5R7P5	Inositol-1-monophosphatase	IMPA1	0.027	-1.34
A0A1D5QIK3	SAFB like transcription modulator	SLTM	0.027	-0.724
A0A5F8ANH4	Coagulation factor II	F2	0.027	1.11
A0A1D5QZ18	Complement component 8 subunit beta	C8B	0.027	1.26
A0A5F8AKB8	Histone H2B	H2BC17	0.027	3.3
A0A1D5R536	Kinectin 1	KTN1	0.028	-0.864
F6UZ60	Fibrinogen alpha chain	FGA	0.028	1.12
F7HAB9	Golgi associated, gamma adaptin ear containing, ARF binding protein 1	GGA1	0.029	-1.37
F6WIQ0	Uncharacterized protein	SET	0.029	-1.32
A0A5F7ZB67	Pyruvate kinase	PKLR	0.029	0.721
A0A1D5R9K8	Microfibril associated protein 4	MFAP4	0.029	0.828
A0A1D5QPA5	KH-type splicing regulatory protein	KHSRP	0.03	-0.814
I0FHZ5	Phosphoinositide phospholipase C	PLCD1	0.03	0.748
A0A5F7ZAZ2	C1q domain-containing protein	C1QC	0.03	1.37
A0A5F7ZNS5	Uncharacterized protein	ACOT2	0.03	1.85
A0A1D5QVX8	ATP-dependent (S)-NAD(P)H-hydrate dehydratase	NAXD	0.031	-1.14
A0A5F8A3T7	Ig-like domain-containing protein		0.031	0.79
F7AL41	Formin-binding protein 1-like	FNBP1L	0.032	-0.837
F7GRA6	Complement C8 gamma chain	C8G	0.032	0.7
A0A1D5RJK6	Uncharacterized protein	FUBP1	0.033	-1.07
H9END9	Tropomyosin alpha-4 chain isoform 2	TPM4	0.033	-0.624
A0A5F7ZEZ9	Fibrinogen beta chain	FGB	0.034	1.72
A0A5F7ZFX7	Fructose-bisphosphatase	FBP2	0.035	-1.25
A0A5F7ZJW9	Uncharacterized protein	MANF	0.035	-0.838
F6YBP7	Adipsin	CFD	0.035	1.03

Table 1 (continued)

Accession Number	Protein name	Gene name	*p*-value	Log2 Aged Rhesus
H9Z3B8	Copper transport protein ATOX1	ATOX1	0.036	-0.942
A0A1D5R0N5	Uncharacterized protein	MYL6	0.036	0.572
A0A1D5Q833	PTPRF interacting protein alpha 1	PPFIA1	0.037	-1.02
A0A1D5QJR4	Host cell factor C1	HCFC1	0.039	-1.04
F7GXX7	Small ubiquitin-related modifier	SUMO1P1	0.039	-0.968
A0A1D5QFS4	Scaffold attachment factor B	SAFB	0.039	-0.889
F7APH2	Heterogeneous nuclear ribonucleoprotein D0 isoform c	HNRNPD	0.039	-0.556
F6T0W5	Tetranectin	CLEC3B	0.04	0.803
F6QQP0	Uncharacterized protein		0.041	0.737
A0A1D5QMN6	Serpin family B member 6	SERPINB6	0.042	-0.577
F6SJD2	CXXC motif containing zinc binding protein	CZIB	0.042	0.678
A0A5F7ZI29	Uncharacterized protein	JCHAIN	0.042	0.731
F6TQ14	Carbonic anhydrase	CA2	0.042	0.92
F7F874	Thiamine pyrophosphokinase	TPK1	0.043	-1.18
F7FF62	Proteasome activator complex subunit 1 isoform 1	PSME1	0.043	-0.76
A0A5F7ZKJ3	Pyruvate dehydrogenase phosphatase regulatory subunit	PDPR	0.043	1.06
F7HNR1	Anterior gradient 2, protein disulphide isomerase family member	AGR2	0.043	2.74
H9FXA8	Proteasome subunit alpha type	PSMA7	0.044	-0.848
A0A1D5QYN2	Glutathione reductase	GSR	0.044	-0.611
I0FNJ1	Epididymal secretory protein E1	NPC2	0.045	-0.777
F7FLX2	GDP-4-keto-6-deoxy-D-mannose-3,5-epimerase-4-reductase	GFUS	0.045	0.503
F7F6K7	Junctional cadherin 5 associated	JCAD	0.046	-2.05
A0A5F8ATC0	Eukaryotic translation initiation factor 2 subunit beta	EIF2S2	0.046	-0.827
A0A1D5QSC4	Epidermal growth factor receptor pathway substrate 15	EPS15	0.046	-0.703
A0A5F8A837	Uncharacterized protein	SUGT1	0.046	-0.563
F7F2A5	Metavinculin	VCL	0.046	-0.5
F7HER2	Actinin alpha 3	ACTN3	0.048	-0.771
G7MLE5	Phosphoglycerate mutase	PGAM2	0.048	-0.542
F7E3N5	Phosphatase domain containing paladin 1	PALD1	0.048	-0.524
A0A5F8ATN0	Histone H2A	H2AZ2	0.048	2.66
A0A5F8AJ37	RAB8B, member RAS oncogene family	RAB8B	0.049	-0.55
F7H4P3	Proteasome subunit beta	PSMB4	0.05	-0.804
A0A5F7ZMU2	Uncharacterized protein	CFHR5	0.05	0.766

The last two proteins downregulated in both rhesus macaques and olive baboons (aged *vs.* young) were: heterogeneous nuclear ribonucleoprotein D0 [HNRNPD (RM -0.556/OB -0.604)], which binds to heterogenous nuclear RNA (hnRNA) and is thought to prevent age-related neurodegenerative diseases [30], has been found under expressed in COVID-19 patients, further supporting interactions of SARS-CoV-2 with host factors [31]. Finally, Serpin B6 [SERPINB6 (RM -0.577/OB -1.4)] is a serine protease inhibitor and its downregulation is associated with increased SARS-CoV-2 uptake and replication [32], which could explain the higher COVID-19 pathology observed in aged infected animals.

Lastly, we found a few other DAPs (aged *vs.* young) that were shared by rhesus macaques and olive baboons but only significant ($\log_2$ fold change $\leq$ -0.5 or $\geq$ 0.5 and p-value $<$ 0.05) in one of these two NHP species. Among the ones over expressed, we found Desmoplakin [DSP (RM 0.444/

Table 2 List of DAPs for olive baboons (aged *vs.* young). Accession number, protein name, gene name, *p*-value and $\log_2$ Fold Change are provided. Proteins are ordered by increasing *p*-value. Top 5 DAPs are highlighted in bold

Accession number	Protein name	Gene name	*p*-value	Log2 aged baboon
A0A096NQN2	**Pentraxin**	**APCS**	**< 0.0001**	**2.99**
A0A096NEV9	**Ig-like domain-containing protein**	**IGHA**	**< 0.0001**	**1.84**
A0A2I3M4W7	**Dematin actin binding protein**	**DMTN**	**0.00013**	**1.41**
A0A2I3MAI1	**Transketolase**	**TKT**	**0.00023**	**-0.63**
A0A096N1Y1	**Clusterin**	**CLU**	**0.00029**	**0.787**
A0A2I3MM55	Joining chain of multimeric IgA and IgM	JCHAIN	0.00038	1.78
A0A2I3MW37	Paraspeckle component 1	PSPC1	0.0004	-1.91
A0A096P228	Complement C4-A	C4A	0.00042	1.29
A0A096NJK4	Serpin family A member 3	SERPINA3	0.00043	1.38
A0A2I3MWE6	Ig-like domain-containing protein	IGHM	0.00062	1.35
A0A2I3LD62	Transcription elongation regulator 1	TCERG1	0.00068	-1.37
A0A2I3N2B9	IGv domain-containing protein		0.00071	1.25
A0A096NIN4	Cell division cycle 5 like	CDC5L	0.00071	1.17
A0A096MM00	Non-POU domain containing octamer binding	NONO	0.00075	-1.8
A0A096NN03	HDGF like 3	HDGFL3	0.00084	2.74
A0A2I3NEJ3	Laminin subunit beta 2	LAMB2	0.0009	0.731
A0A096NUT9	RALY heterogeneous nuclear ribonucleoprotein	RALY	0.0011	-0.892
A0A2I3LWK4	Immunoglobulin heavy variable 3–72	IGHV3-72	0.0012	1.46
A0A0A0MUA3	Heterogeneous nuclear ribonucleoprotein M	HNRNPM	0.0012	-1.43
A0A096MPI8	Filaggrin family member 2	FLG2	0.0013	2.12
A0A096NSI5	Calretinin	CALB2	0.0015	2.43
A0A096N317	Splicing factor, proline- and glutamine-rich	SFPQ	0.0015	-1.15
A0A2I3MJZ3	Actinin alpha 2	ACTN2	0.0015	-1.44
A0A2I3MDY2	Myocardin related transcription factor B	MRTFB	0.0016	-1.48
A0A0A0MU60	Aldehyde dehydrogenase family 16 member A1	ALDH16A1	0.0017	1.93
A0A2I3NGY5	Ig-like domain-containing protein		0.0017	1.16
A0A2I3NC97	Ig-like domain-containing protein		0.0017	1
A0A2I3MP06	Tropomyosin 4	TPM4	0.0017	0.55
A0A2I3M158	Ubiquitin recognition factor in ER associated degradation 1	UFD1	0.0017	-1.87
A0A0A0MU58	Actinin alpha 4	ACTN4	0.002	-1.56
A0A2I3LZX6	Uncharacterized protein	HNRNPH2	0.0021	-1.79
P05770	Apolipoprotein E	APOE	0.0023	1.39
A0A2I3M2P0	Heterogeneous nuclear ribonucleoprotein H1	HNRNPH1	0.0023	-1.65
A0A096N1T1	Histidine rich glycoprotein	HRG	0.0024	0.801
A0A2I3MT71	Complement C1r subcomponent like	C1RL	0.0025	1.36
A0A2I3LTI2	General vesicular transport factor p115	USO1	0.0028	-1.17
A0A096NKK0	Serpin family B member 9	SERPINB9	0.0029	-1.07
A0A2I3MTT7	Ribosomal protein L22	RPL22	0.0029	-1.69
A0A096NK84	Cysteine rich protein 1	CRIP1	0.0032	1.95
A0A2I3LU29	PC4 and SFRS1 interacting protein 1	PSIP1	0.0032	1.09
A0A096P0K3	Spectrin alpha, non-erythrocytic 1	SPTAN1	0.0033	-0.771
A0A2I3MTE9	Ig-like domain-containing protein		0.0035	1.36
A0A2I3M360	Inter-alpha-trypsin inhibitor heavy chain 5	ITIH5	0.0036	-0.971
A0A2I3LFB9	Zinc finger protein 207	ZNF207	0.0036	-0.985
A0A2I3M0F1	Lymphocyte cytosolic protein 2	LCP2	0.0037	1.65

Table 2 (continued)

Accession number	Protein name	Gene name	*p*-value	Log2 aged baboon
A0A2I3MCZ4	Ig-like domain-containing protein		0.0044	0.832
A0A2I3LP09	Shisa family member 7	SHISA7	0.0048	-0.728
A0A0A0MU78	Shisa family member 7	SHISA7	0.0048	-0.749
A0A096N709	Transaldolase	TALDO1	0.0048	-0.771
A0A096N345	Hemopexin	HPX	0.0049	0.689
A0A2I3LXY2	Non-specific serine/threonine protein kinase	SLK	0.005	-1
A0A2I3LHU4	HLA class II histocompatibility antigen, DR beta 3 chain		0.0054	4.55
A0A096N4D7	Ro60, Y RNA binding protein	RO60	0.0057	-0.627
A0A2I3LMG7	Spectrin alpha, non-erythrocytic 1	SPTAN1	0.0057	-0.978
A0A096NFT8	MARCKS like 1	MARCKSL1	0.0059	1.75
A0A2I3N4Y0	Calumenin	CALU	0.006	1.65
A0A2I3LNH3	KH-type splicing regulatory protein	KHSRP	0.006	-0.719
A0A096P4D3	Multimerin 2	MMRN2	0.0061	0.851
A0A2I3LJS5	Myosin heavy chain 10	MYH10	0.0062	-0.923
A0A2I3NAA8	Apoptosis inducing factor mitochondria associated 1	AIFM1	0.0062	-1.3
A0A096N7V3	Complement component 4 binding protein alpha	C4BPA	0.0063	1.33
A0A2I3M1T5	Adenosine deaminase RNA specific	ADAR	0.0066	-0.934
A0A2I3MSR7	Tropomyosin 3	TPM3	0.0067	0.647
A0A2I3MIX0	DNA damage-binding protein 1	DDB1	0.0067	-0.627
A0A096MYE5	Myosin regulatory light chain 12A	MYL12A	0.0068	0.914
A0A096NL32	Enoyl-CoA delta isomerase 1	ECI1	0.0068	-2.39
A0A2I3MZY8	Aldo–keto reductase family 1 member C1 homolog	AKR1C1	0.0069	-1.09
A0A2I3MSB6	Cytochrome b-c1 complex subunit 7	UQCRB	0.0075	3.13
A0A2I3LPQ6	CXADR Ig-like cell adhesion molecule	CXADR	0.0076	1.06
A0A096MWL2	Syndecan binding protein	SDCBP	0.0076	0.622
A0A2I3M6Q6	Nuclear mitotic apparatus protein 1	NUMA1	0.0077	-0.665
A0A2I3LE24	PTPRF interacting protein alpha 1	PPFIA1	0.0077	-0.696
A0A2I3LH89	Ig-like domain-containing protein		0.0078	1.12
A0A096P0S3	V-type proton ATPase subunit G	ATP6V1G1	0.0079	3.14
A0A096NBS2	Selenocysteine lyase	SCLY	0.0085	-0.526
A0A096NZE2	Small RNA binding exonuclease protection factor La	SSB	0.0086	-1.61
A0A096NFU9	Ig-like domain-containing protein		0.0088	2.54
A0A096NV22	Endoplasmic reticulum oxidoreductase 1 alpha	ERO1A	0.009	0.597
A0A096NRJ1	CD59 glycoprotein		0.009	0.56
A0A096P5I3	Keratin 27	KRT27	0.0092	1.13
A0A2I3LH21	Dynein cytoplasmic 1 intermediate chain 2	DYNC1I2	0.0096	-1.36
A0A2I3M314	QKI, KH domain containing RNA binding	QKI	0.0098	-1.41
A0A2I3N4K0	G3BP stress granule assembly factor 1	G3BP1	0.01	1.28
A0A096N6A0	Myristoylated alanine rich protein kinase C substrate	MARCKS	0.01	0.988
A0A2I3N200	Heterogeneous nuclear ribonucleoprotein D	HNRNPD	0.01	-0.604
A0A096P2E8	Nuclear cap-binding protein subunit 3	NCBP3	0.011	1.44
A0A096NM11	Ig-like domain-containing protein		0.011	1.35
A0A2I3MSK0	Nucleoporin 153	NUP153	0.011	-1.4
A0A2I3LID9	RNA binding protein fox-1 homolog 1	RBFOX1	0.011	-1.42
B0VYX8	Cytochrome c oxidase subunit 5A, mitochondrial	COX5A	0.012	0.938
A0A2I3LRD7	Laminin subunit alpha 3	LAMA3	0.012	0.93

Table 2 (continued)

Accession number	Protein name	Gene name	*p*-value	Log2 aged baboon
A0A096NT92	Galectin-3-binding protein	LGALS3BP	0.012	0.553
A0A096N5V4	Chitinase-3-like protein 1	CHI3L1	0.012	-1.2
A0A2I3MZJ5	Talin 1	TLN1	0.013	-0.643
A0A2I3M4M4	Cell division cycle and apoptosis regulator 1	CCAR1	0.013	-1.34
A0A2I3MIF7	Filamin-C	FLNC	0.014	-1.84
A0A0A0MWY7	Splicing factor U2AF subunit	U2AF2	0.014	-1.89
A0A096MQP5	Ig-like domain-containing protein		0.015	1.57
A0A096NVY7	BH3-interacting domain death agonist	BID	0.015	0.966
A0A096NEY1	Choline-specific glycerophosphodiester phosphodiesterase	ENPP6	0.015	-1.75
A0A096NKT3	Desmoplakin	DSP	0.016	0.618
A0A096MNQ3	C-X-C motif chemokine	PPBP	0.016	-0.575
A0A2I3MIV3	Actinin alpha 1	ACTN1	0.016	-1.13
A0A0A0MXC4	Transcription elongation factor SPT5	SUPT5H	0.016	-1.23
A0A096MPU5	Serpin B6-like	SERPINB6	0.016	-1.4
A0A2I3LKR9	Septin	SEPTIN11	0.016	-1.43
A0A2I3M614	Keratin, type I cuticular Ha3-I	KRT33A	0.017	1.53
A0A0A0MWZ3	Calponin	CNN1	0.017	1.03
A0A2I3LNI7	Acidic nuclear phosphoprotein 32 family member A	ANP32A	0.017	1.02
A0A096N402	Cathepsin D	CTSD	0.017	0.545
A0A096N9Y0	Clathrin interactor 1	CLINT1	0.017	-0.729
A0A2I3M3R5	Prefoldin subunit 4	PFDN4	0.018	1.82
A0A096NUK6	Myosin light chain 9	MYL9	0.018	0.841
A0A2I3MGL1	Solute carrier family 12 member 2	SLC12A2	0.018	0.783
A0A2I3NB00	EPS8 like 2	EPS8L2	0.018	-0.57
A0A0A0MUI0	Tripartite motif containing 28	TRIM28	0.018	-0.869
A0A2I3N473	60S ribosomal protein L8	RPL8	0.018	-1.88
A0A2I3MQY3	Immunoglobulin kappa variable 4–1	IGKV4-1	0.019	0.84
A0A096N1J7	Apolipoprotein D	APOD	0.019	0.617
A0A096NFB0	All-trans-retinol dehydrogenase [NAD(+)] ADH1B	ADH7	0.019	-0.898
A0A096MWK3	Filamin A	FLNA	0.019	-0.938
A0A096N6E3	Hyaluronan and proteoglycan link protein 1	HAPLN1	0.019	-2.56
A0A2I3LE14	Keratin 10	KRT10	0.02	1.03
A0A096N0H9	Adducin 2	ADD2	0.02	0.514
A0A096N1Y4	PKSO	ADH7	0.02	-0.795
A0A2I3MZ49	Serine and arginine rich splicing factor 5	SRSF5	0.021	2.9
A0A2I3MDH7	Serine and arginine rich splicing factor 10	SRSF10	0.021	1.68
A0A096N0E7	Marginal zone B and B1 cell specific protein	MZB1	0.021	1.35
A0A096N6Z6	Poly(rC) binding protein 1	PCBP1	0.021	-1.09
A0A096NA79	Transcription factor Sp1	SP1	0.021	-1.52
A0A096MU45	Ig-like domain-containing protein		0.022	1.1
A0A2I3MM66	Protein S100 TYMP	S100A11	0.022	0.506
A0A096MN47	Keratin 77	KRT77	0.023	1.08
A0A2I3LS05	2-phospho-D-glycerate hydro-lyase	ENO2	0.023	-0.942
A0A096MVE7	RWD domain containing 1	RWDD1	0.024	1.3
A0A2I3N9B6	Host cell factor C1	HCFC1	0.024	-0.707

Table 2 (continued)

Accession number	Protein name	Gene name	*p*-value	Log2 aged baboon
A0A2I3LXU6	Ribosomal protein	RPL10A	0.024	-1.16
A0A2I3MXU2	Synaptotagmin binding cytoplasmic RNA interacting protein	SYNCRIP	0.024	-1.19
A0A2I3M825	Zinc finger RNA binding protein	ZFR	0.024	-1.31
A0A2I3M8L5	Synaptopodin 2	SYNPO2	0.025	1.58
A0A2I3M1I3	Latent transforming growth factor beta binding protein 1	LTBP1	0.025	0.972
A0A096MV46	Immunoglobulin kappa variable 6D-41 (non-functional)	IGKV6D-41	0.025	0.764
A0A096NR90	Ig-like domain-containing protein		0.026	1.04
A0A2I3MML7	Ig-like domain-containing protein		0.026	0.842
A0A2I3LKS6	Tight junction protein 1	TJP1	0.026	-0.559
A0A096P3B1	Aldo–keto reductase family 1 member C1 homolog	AKR1C1	0.026	-1.05
A0A2I3MLZ3	Seryl-tRNA synthetase	SARS1	0.026	-1.3
A0A096N2S9	F-spondin	SPON1	0.026	-1.47
A0A096MYJ5	Copine 3	CPNE3	0.027	0.539
A0A096NAR9	Spectrin beta chain	SPTBN1	0.028	-0.624
A0A096N5A4	HtrA serine peptidase 2	HTRA2	0.029	0.528
A0A2I3LNW4	Tight junction protein 2	TJP2	0.029	-0.729
A0A096MNW7	Adipocyte-type fatty acid-binding protein	FABP4	0.029	-1.23
A0A2I3N8Y4	3-beta-hydroxysterol Delta (14)-reductase	LBR	0.031	1.79
A0A2I3LFF0	Keratin 17	KRT17	0.031	1.67
A0A096P1P8	Frataxin, mitochondrial	FXN	0.031	0.969
A0A2I3LJL3	Non-specific protein-tyrosine kinase	PTK2	0.031	-0.525
A0A2I3MM96	Heat shock protein family A (Hsp70) member 5	HSPA5	0.031	-1.87
A9L8U0	Hemoglobin subunit theta 1	HBQ1	0.032	1.51
A0A2I3N512	4-trimethylaminobutyraldehyde dehydrogenase	ALDH9A1	0.032	0.727
A0A2I3LIT0	GLI pathogenesis related 2	GLIPR2	0.032	-0.513
A0A096N1H4	Splicing factor 3b subunit 1	SF3B1	0.032	-0.9
A0A0A0MWU1	Bromodomain containing 4	BRD4	0.032	-0.965
A0A096N5N8	Uncharacterized protein	HNRNPA3	0.032	-2.26
A0A096P131	Acidic nuclear phosphoprotein 32 family member B	ANP32B	0.034	0.83
A0A096P5P4	Junction plakoglobin	JUP	0.034	0.652
A0A096ML84	Uncharacterized protein	HNRNPA3	0.034	-1.94
A9X1C4	Huntingtin interacting protein K	HYPK	0.035	1.06
A0A096NPT5	Heterogeneous nuclear ribonucleoprotein A3	HNRNPA3	0.036	-1.15
A0A096MXZ5	Serine and arginine rich splicing factor 9	SRSF9	0.037	0.767
A0A096NZG7	ADP-ribosyl cyclase/cyclic ADP-ribose hydrolase	BST1	0.037	0.509
A0A2I3M5I3	Small nuclear ribonucleoprotein U5 subunit 200	SNRNP200	0.037	-0.749
A0A2I3LIJ2	Septin	SEPTIN7	0.037	-0.873
A0A096N4V8	Keratin, type II cytoskeletal 6C	KRT5	0.039	1.18
A0A2I3M017	Parvalbumin	PVALB	0.039	0.543
A0A096MV19	Thyroid hormone receptor associated protein 3	THRAP3	0.039	-0.742
A0A096P4S7	Serine/arginine-rich splicing factor 1	SRSF1	0.04	0.871
A0A2I3N6J2	Tensin 1	TNS1	0.041	-0.64
A0A096MQV4	Lamin A/C	LMNA	0.041	-1.16
A0A2I3MZ19	RNA binding protein, mRNA processing factor	RBPMS	0.042	1.23
A0A096NDH2	CSD domain-containing protein	YBX1	0.042	1.16
A0A2I3LXT9	PDS5 cohesin associated factor B	PDS5B	0.042	-0.97

Table 2 (continued)

Accession number	Protein name	Gene name	*p*-value	Log2 aged baboon
A0A096N233	Taxilin alpha	TXLNA	0.043	4.23
A0A096NUU1	Charged multivesicular body protein 4B	CHMP4B	0.043	1
A0A2I3MLK1	Pinin	PNN	0.044	-1.18
A0A2I3M0D0	Zinc finger CCCH-type containing 11A	ZC3H11A	0.044	-1.45
A0A2I3N574	RRM domain-containing protein	RBMX	0.045	1.21
A0A2I3M706	Ig-like domain-containing protein		0.045	0.556
A0A096P534	Phenazine biosynthesis like protein domain containing	PBLD	0.045	-1.28
A0A096NPS7	All-trans-retinol dehydrogenase [NAD(+)] ADH1B	ADH7	0.045	-1.32
A0A2I3LFE6	Four and a half LIM domains 1	FHL1	0.046	-1.39
A0A096NWE1	Crystallin beta-gamma domain containing 3	CRYBG3	0.046	-2.76
A4K2N4	Syndecan	SDC4	0.047	1.13
A0A2I3LK27	Moesin	MSN	0.047	-0.711
A0A096NZQ0	Ferredoxin 1	FDX1	0.048	0.929
A0A2I3MLU1	CDKN2A interacting protein	CDKN2AIP	0.048	-1.8
A0A096ML57	Acyl-CoA dehydrogenase family member 8	ACAD8	0.049	0.877
A0A096NAU0	Cytokeratin-1	KRT1	0.049	0.8
A0A2I3N6R9	Heterogeneous nuclear ribonucleoprotein R	HNRNPR	0.049	-0.897
A0A2I3LZ61	Vitelline membrane outer layer 1 homolog	VMO1	0.049	-0.906
A0A096N6J5	Calcium-activated chloride channel regulator 1	CLCA1	0.049	-1.57
A0A2I3LNR5	Amyloid beta precursor like protein 2	APLP2	0.05	1.59
A0A2I3MNR7	Helix-destabilizing protein	HNRNPA1	0.05	-1.35

OB 0.618)] and Junction plakoglobin [JUP (RM 0.0392/OB 0.652)], significantly upregulated in aged olive baboons. These are structural proteins of the cardiac desmosome and intermediate filaments. DSP has been described as a major player in aging lung diseases [33], and is potentially associated with viral myocarditis [34], while levels of JUP were altered in COVID-19 recovered patients with long-term cardiac dysfunction [35]. Also associated with the potential to cause cardiac disease, Tropomyosin alpha-4 chain [TPM4 (RM 0.0628/OB 0.55)] is a common autoantigen in humans identified as part of the COVID-19 autoimmunogenicity repertoire [36]. We also found Clusterin [CLU (RM 0.307/OB 0.787)], which will be discussed in the next section.

Among the ones under expressed, Latent-transforming growth factor beta-binding protein 4 [LTBP4 (RMs -1.24/OB—0.218)] is a regulator of TGFβ signaling, and it has recently emerged as a driver of age-related organ pathologies in a mitochondrial-dependent manner [37]. It was previously found decreased in COVID-19 lung autopsy specimens [38]. Further, Far Upstream element-Binding Protein 1 [FUBP1 (RM -1.07/OB -0.441)] is a master regulator of cell function with oncogenic associations as a dual-agent [39]. Downregulated FUBP1 is associated with higher risk of COVID-19 due to its antiviral function, which may be contributing to increased disease severity in aged NHPs [40]. Next, Alpha-actinin-1 [ACTN1 (RM -0.223/OB -1.13)], a cytoskeleton protein implicated in inflammatory and degenerative autoimmune diseases, is shown to interact with SARS-CoV-2 proteins. Indeed, upregulation of related protein Alpha-actinin-4 results in a protective response to COVID-19 [41], suggesting that downregulation of Alpha-actinin-1 could be associated with disease susceptibility. Finally, Bromodomain-containing protein 4 [BRD4 (RM -0.176/OB -0.965)], an epigenetic regulator with multifaceted roles in aging-related diseases [42], has been associated with the cardiac cytokine storm during SARS-CoV-2 infection [43].

Overall, these results suggest the dysregulation of several immune processes in aged NHPs during SARS-CoV-2 infection, and provide clues of potential host factors that might be associated with increased susceptibility as we age.

Top DAPs in SARS-CoV-2 infected lung tissues from aged vs. young rhesus macaques and olive baboons

We next explored significant species-specific DAPs in aged *vs.* young SARS-CoV-2 infected rhesus macaques (Table 1, Suppl. Fig S1A) and aged *vs.* young SARS-CoV-2 infected olive baboons (Table 2, Suppl. Fig S1B) (p-value < 0.05, absolute $\log_2$ fold change > 0.5) (Fig. 1).

The top five DAPs based on p-value for rhesus macaques were (gene name, $\log_2$ fold change, Accession #) (Table 1, Suppl. Fig S1A): calpain 5 (CAPN5, 1.45, F7EDT3), Protein-Tyrosine phosphatase receptor J (PTPRJ,—0.771, F6TSU2), pentraxin (APCS, 1.14, F7H1V9), heme-binding protein 1 (HEBP1, 1.46, F6UQB6) and t-SNARE coiled-coil homology domain-containing protein (PPP1R8, -0.644, F6V089). Calpains are calcium-activated proteases involved in apoptosis, cell proliferation and motility, and overactivation has been previously associated with aging diseases and pathological lung conditions [44, 45]. SARS-CoV-2 appears to activate calpains, resulting in increased cell death, and their inhibition has been studied as a means of stopping COVID-19 related cytokine storm, inflammation, and pulmonary fibrosis [46–48]. Thus, upregulation of calpain 5 could be involved in the increased disease severity observed in aged NHPs. PTPRJ contributes to protein dephosphorylation, with roles in cell adhesion, migration, proliferation and differentiation, as well as regulation of a variety of immune cells. Downregulation of PTPRJ, as observed here, has been associated with numerous diseases, such as idiopathic pulmonary fibrosis [49]. Indeed, pulmonary fibrosis is one of the long-term consequences of COVID-19 [50]. Thus, under expression of PTPRJ in aged rhesus macaques could indicate an increased potential for developing post-COVID conditions. PTPRJ has also been shown to interact with SARS-CoV-2 ORF3a [51]. Regarding immune effector pentraxin or serum amyloid P component, which was over expressed in aged rhesus macaques, elevated levels of pentraxin 3 have been associated with COVID-19 severity and mortality, and it has been proposed as a promising biomarker for long COVID [52]. Next, HEBP1 has high affinity for heme and porphyrins modulating mitochondrial dynamics, and has been linked to synaptic vulnerability during aging [53]. Its metabolism is interfered by SARS-CoV-2 [54]. Finally, no association has been shown between PPP1R8 and COVID-19.

The top five DAPs based on p-value for olive baboons were (Gene name, Log_2 Fold Change, Accession #) (Table 2, Suppl. Fig. S1B): pentraxin (APCS, 2.99, A0A096NQN2), also a top upregulated DAP in RMs (see above), immunoglobulin heavy constant alpha (IGHA, 1.84, A0A096NEV9), dematin (DMTN, 1.41, A0A2I3M4W7), Transketolase (TKT, -0.63, A0A2I3MAI1), and clusterin (CLU, 0.787, A0A096N1Y1). The over expression of IGHA in aged baboon lungs found here is consistent with the basal increase seen during aging in humans [55]. Although IgA plays an important role during early SARS-CoV-2 neutralization [56], hyperactivation can result in IgA-mediated diseases and has been linked to post-COVID conditions [57], suggesting again that risk of developing long COVID is increased as we age. Dematin, a cytoskeleton-associated protein with functions in formation, bundling and stabilization of F-actin, was also over expressed in aged baboons. Interestingly, there was increased phosphorylation of dematin in patients with post-COVID-19 interstitial lung changes associated with upregulation of proinflammatory immune signatures [58], suggesting an altered immune response during aging. Conversely, transketolase, and enzyme that connects the pentose phosphate pathway to glycolysis, was under expressed in aged infected baboons, although reports indicate that SARS-CoV-2 infection upregulates transketolase levels [59]. Lastly, clusterin is a glycoprotein that functions as a stress-activated and ATP-independent molecular chaperone. It is predicted to be a strong interactor of ACE2 receptor**,** and was found increased in the lungs of coronavirus-infected individuals [60], in agreement with our observations in aged baboons. Interestingly, it seems that cellular localization of clusterin (intra- or extracellular) leads to divergent effects on epithelial cell regeneration and lung repair during fibrosis, with both beneficial and detrimental roles [61], although its role during COVID-19 is yet to be understood.

Overall, several of the factors found differentially expressed in aged NHPs seem to play a role in the development of post-COVID diseases, in agreement with a greater risk of persisting symptoms associated with COVID-19 among older people (65 + years) [62].

Pathway analysis in aged NHPs

We further explored pathways relevant to SARS-CoV-2 infection focusing in aged NHPs. We identified nine common pathways enriched in both NHP species studied (Fig. 2 and Table 3). Based on the calculated IPA Z-scores, the ones with reduced activation were Paxillin signaling, Leukocyte Extravasation signaling, VEGF signaling, Actin cytoskeleton signaling, and Integrin signaling. The ones with increased activation were GP6 signaling pathway and LXR/RXR activation. We also identified two divergent pathways: Protein kinase A signaling (activation increased in rhesus macaques but decreased in olive baboons) and Ferroptosis signaling (activation decreased in rhesus macaques but increased in olive baboons) pathways.

Most of these pathways have been previously associated with COVID-19. Indeed, disruption of the VEGF-related pathways was previously seen during both acute and long COVID-19 [63], in agreement with our observations. Further, disruption of the host actin cytoskeleton, as seen here, is tightly connected to pathological processes during SARS-CoV-2 infection, where the virus highjacks cytoskeletal functions leading to increased viral loads, dissemination, and immune dysfunction [64]. Conversely, while integrin activation is essential for SARS-CoV-2 infection [65], we found reduced integrin signaling in aged NHPs. Indeed, it has been shown that inflammatory cytokines activate certain integrins, promoting cellular adherence to counter-receptors such as ICAMs resulting in phagocytosis and cytotoxic killing [66]. Low integrin signaling in the elderly could potentially be associated to decreased killing and thus, increased susceptibility to infections. In addition, activation of the GP6 pathway was observed in whole blood from COVID-19 patients and its upregulation constituted a molecular signature for COVID-19 progression and severity [67, 68], indicating a potential link with the increased pathology observed in aged NHPs. Next, the liver X receptor/retinoid X receptor or LXR/RXR activation pathway, which plays a key role in the regulation of cholesterol, lipid metabolism, and inflammation, was found enriched here

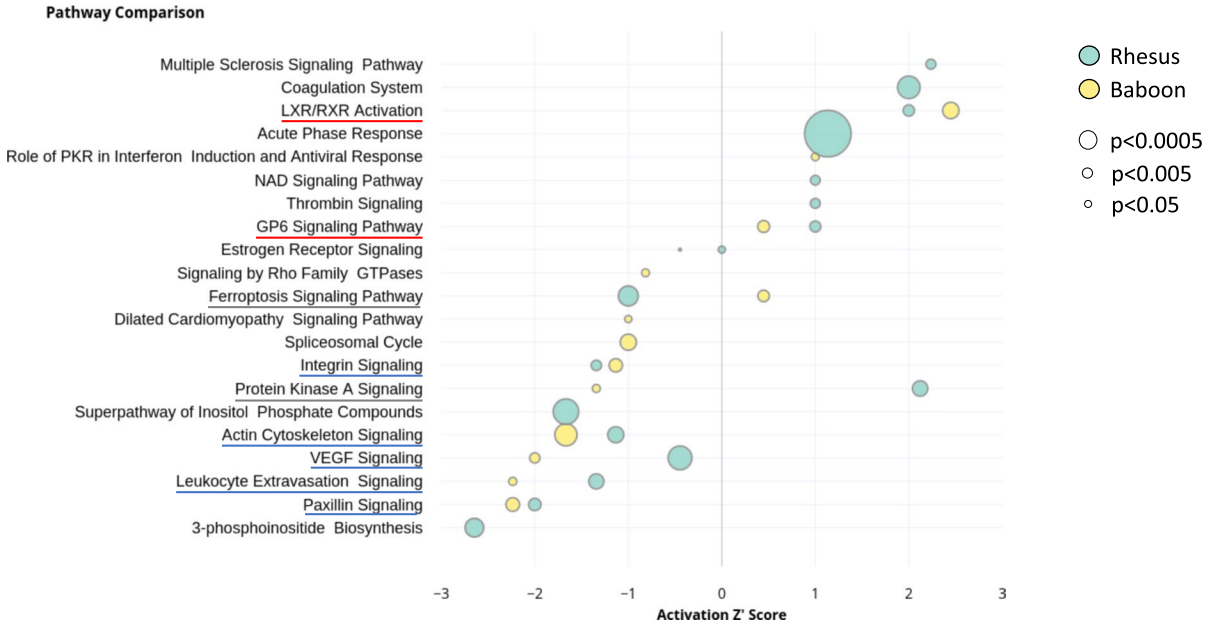

Fig. 2 Comparison of top 21 canonical pathways in aged rhesus macaques and aged olive baboons. Rhesus macaques (cyan) and olive baboons (yellow) activation Z-scores (an inferred measurement of the pathway activation stated based on measured levels and IPA knowledge) is shown by bubble position on the X-axis, pathway names in the Y-axis, where *p*-values are represented by bubble size. Highly overlapping pathways were removed from analysis and only the most comprehensive pathway is displayed. Enriched pathways in both rhesus macaques and olive baboons are underlined in red (increased activation), blue (reduced activation), or grey (divergent)

Table 3 Comparison of canonical pathways in aged rhesus macaques and aged olive baboons. List of all pathways reported in IPA, with pathway activation z-score and -log *p*-values provided for the ones detected in old rhesus macaques and old olive baboons. Pathways are ordered by activation trend and are considered significantly enriched if -log (*p*-value) > 1.3 (equivalent to *p*-value < 0.05). Enriched pathways in both NHP species are highlighted in bold

Canonical pathways	Rhesus z-score	Baboon z-score	Rhesus -log *p*-value	Baboon -log *p*-value
LXR/RXR Activation	2.0000	2.4490	2.0803	3.0287
Paxillin Signaling	-2.0000	-2.2360	2.2914	2.5223
Leukocyte Extravasation Signaling	-1.3420	-2.2360	2.7958	1.4927
Protein Kinase A Signaling	2.1210	-1.3420	2.8470	1.4524
Actin Cytoskeleton Signaling	-1.1340	-1.6670	2.9773	4.0654
D-myo-inositol (1,4,5,6)-Tetrakisphosphate Biosynthesis	-2.6460	N/A	3.7825	0.0000
D-myo-inositol (3,4,5,6)-tetrakisphosphate Biosynthesis	-2.6460	N/A	3.7825	0.0000
3-phosphoinositide Degradation	-2.6460	N/A	3.6098	0.0000
3-phosphoinositide Biosynthesis	-2.6460	N/A	3.4238	0.0000
Integrin Signaling	-1.3420	-1.1340	1.9137	2.4694
VEGF Signaling	-0.4470	-2.0000	4.3537	1.8903
Multiple Sclerosis Signaling Pathway	2.2360	N/A	1.8347	0.0000
Intrinsic Prothrombin Activation Pathway	2.0000	N/A	3.8150	0.4957
Coagulation System	2.0000	N/A	4.1297	0.5618
Superpathway of Inositol Phosphate Compounds	-1.6670	N/A	4.6609	0.0000
D-myo-inositol-5-phosphate Metabolism	-1.6670	N/A	N/A	N/A
Ferroptosis Signaling Pathway	-1.0000	0.4470	3.6630	2.1370
GP6 Signaling Pathway	1.0000	0.4470	2.0326	2.2068
Acute Phase Response Signaling	1.1340	N/A	8.5300	N/A
MicroRNA Biogenesis Signaling Pathway	0.0000	-1.1340	N/A	N/A
Spliceosomal Cycle	N/A	-1.0000	0.0000	2.9871
EIF2 Signaling	0.0000	-1.0000	N/A	N/A
Thrombin Signaling	1.0000	N/A	1.8118	0.4724
Dilated Cardiomyopathy Signaling Pathway	N/A	-1.0000	0.5990	1.3127
Complement System	1.0000	N/A	N/A	N/A
NAD Signaling Pathway	1.0000	N/A	1.7796	0.3971
Role of PKR in Interferon Induction and Antiviral Response	N/A	1.0000	0.6606	1.4429
RHOA Signaling	N/A	-0.8160	N/A	N/A
Signaling by Rho Family GTPases	N/A	-0.8160	0.2883	1.4431
ILK Signaling	0.0000	-0.7070	N/A	N/A
Apoptosis Signaling	N/A	-0.4470	N/A	N/A
Estrogen Receptor Signaling	0.0000	-0.4470	1.3055	0.4987
Asparagine Degradation I	N/A	N/A	1.8914	0.0000
Agranulocyte Adhesion and Diapedesis	N/A	N/A	0.8124	1.3602
D-myo-inositol (1,4,5)-Trisphosphate Biosynthesis	N/A	N/A	1.9170	0.0000
Virus Entry via Endocytic Pathways	N/A	N/A	0.7534	2.3407
IL-33 Signaling Pathway	N/A	N/A	2.1435	0.0000
Sertoli Cell-Sertoli Cell Junction Signaling	N/A	N/A	N/A	N/A
Protein Ubiquitination Pathway	N/A	N/A	2.0631	0.3427
Myo-inositol Biosynthesis	N/A	N/A	1.4976	0.0000
Production of Nitric Oxide and Reactive Oxygen Species in Macrophages	N/A	N/A	1.4523	0.5971

Table 3 (continued)

Canonical pathways	Rhesus z-score	Baboon z-score	Rhesus -log *p*-value	Baboon -log *p*-value
Role of Tissue Factor in Cancer	N/A	N/A	3.0278	0.0000
Pentose Phosphate Pathway	N/A	N/A	0.0000	2.3660
Gluconeogenesis I	N/A	N/A	N/A	N/A
Tumoricidal Function of Hepatic Natural Killer Cells	N/A	N/A	N/A	N/A
Granzyme B Signaling	N/A	N/A	N/A	N/A
UVA-Induced MAPK Signaling	N/A	N/A	2.4270	0.0000
FAT10 Signaling Pathway	N/A	N/A	N/A	N/A
Remodeling of Epithelial Adherens Junctions	N/A	N/A	N/A	N/A
Extrinsic Prothrombin Activation Pathway	N/A	N/A	N/A	N/A
Regulation of Cellular Mechanics by Calpain Protease	N/A	N/A	N/A	N/A
Noradrenaline and Adrenaline Degradation	N/A	N/A	0.0000	1.3499
Thyroid Hormone Biosynthesis	N/A	N/A	0.0000	1.7413
GDP-L-fucose Biosynthesis I (from GDP-D-mannose)	N/A	N/A	1.8914	0.0000
TCA Cycle II (Eukaryotic)	N/A	N/A	2.0203	0.0000
CSDE1 Signaling Pathway	N/A	N/A	N/A	N/A
Isoleucine Degradation I	N/A	N/A	0.0000	1.9398
Thiamin Salvage III	N/A	N/A	2.1910	0.0000
FXR/RXR Activation	N/A	N/A	N/A	N/A
Apelin Cardiomyocyte Signaling Pathway	N/A	N/A	N/A	N/A
Regulation of eIF4 and p70S6K Signaling	N/A	N/A	1.5330	0.0000
Antigen Presentation Pathway	N/A	N/A	1.5826	0.0000
NADH Repair	N/A	N/A	N/A	N/A
Inhibition of ARE-Mediated mRNA Degradation Pathway	N/A	N/A	N/A	N/A
L-carnitine Biosynthesis	N/A	N/A	0.0000	1.5672
2-ketoglutarate Dehydrogenase Complex	N/A	N/A	1.5931	0.0000
BAG2 Signaling Pathway	N/A	N/A	N/A	N/A
Fatty Acid β-oxidation III (Unsaturated, Odd Number)	N/A	N/A	0.0000	1.4443
Pentose Phosphate Pathway (Non-oxidative Branch)	N/A	N/A	N/A	N/A
Chronic Myeloid Leukemia Signaling	0.0000	N/A	N/A	N/A
Coronavirus Replication Pathway	N/A	N/A	N/A	N/A
Germ Cell-Sertoli Cell Junction Signaling	N/A	N/A	N/A	N/A
Tight Junction Signaling	N/A	N/A	N/A	N/A
Clathrin-mediated Endocytosis Signaling	N/A	N/A	N/A	N/A
Phagosome Maturation	N/A	N/A	N/A	N/A
Insulin Secretion Signaling Pathway	0.0000	N/A	N/A	N/A
Valine Degradation I	N/A	N/A	N/A	N/A
Gap Junction Signaling	N/A	N/A	N/A	N/A
Inosine-5'-phosphate Biosynthesis II	N/A	N/A	N/A	N/A
Ethanol Degradation II	N/A	N/A	0.0000	1.3938
Glycolysis I	N/A	N/A	N/A	N/A
Rapoport-Luebering Glycolytic Shunt	N/A	N/A	N/A	N/A
Glutathione Redox Reactions II	N/A	N/A	N/A	N/A
14–3-3-mediated Signaling	N/A	N/A	N/A	N/A
Death Receptor Signaling	N/A	0.0000	N/A	N/A

Table 3 (continued)

Canonical pathways	Rhesus z-score	Baboon z-score	Rhesus -log *p*-value	Baboon -log *p*-value
PPARα/RXRα Activation	N/A	N/A	N/A	N/A
Iron homeostasis signaling pathway	N/A	N/A	N/A	N/A

as well as in a multi-omics study that linked this pathway to COVID-19 severity [69]. Interestingly, a higher HDL-cholesterol measured before infection was associated with a lower risk of death during COVID-19 in older humans [70]. Lastly, activation of the ferroptosis pathway by SARS-CoV-2 might be associated with COVID-19 cardiovascular complications [71], although we only found increased activation in aged olive baboons (but decreased in rhesus macaques). This could be related to the higher disease pathology observed in baboons compared to rhesus [72].

Other statistically significant pathways were identified in only one of the two NHP species studied and are presented in Suppl. Table S1 (rhesus macaques) and Suppl. Table S2 (olive baboons). In aged rhesus macaques, the top three altered pathways based on p-value were: the Acute Phase Response signaling, the Complement system, and the Extrinsic Prothrombin Activation Pathway. The Acute Phase Response signaling, a rapid inflammatory response that provides protection against microorganisms, was found activated and suggests an overactive immune response in aged NHPs, similar to our observations in elderly humans [73]. The Complement system was also activated, specifically, the Alternative Pathway, which may play a major role in SARS-CoV-2 pathogenesis [74]. Upregulation of both acute phase response signaling and the complement system were previously seen in COVID-19 patients, linking it to IL-6 production, increased inflammation and tissue damage [75, 76]. Finally, the Extrinsic Prothrombin Activation Pathway had a z-score = 0, but with increased levels of fibrin, alpha-thrombin and fibrinogen, as well as coagulation factor II, indicating increased risk of COVID-19-related coagulopathy in aged rhesus macaques, similar to humans [77]. Inhibition of the complement pathway as a therapeutic strategy during COVID-19 resulted in reduced acute-phase reaction and thrombin activity, further linking these three pathways to disease severity [78]. Complete pathway results for rhesus macaques can be found in Suppl. Table S1.

In aged olive baboons, the top three statistically significant enriched pathways based on p-value (with assigned z-score) were: the Actin cytoskeleton signaling, the Integrin-linked kinase (ILK) signaling pathway, and the LXR/RXR signaling pathways. The Actin cytoskeleton signaling was inhibited in both NHP species, as mentioned earlier, suggesting reduced focal adhesion assembly and actin polymerization, like what we observed previously in elderly humans [73]. ILK signaling (closely related to actin cytoskeleton signaling) was also inhibited in aged olive baboons; and the LXR/RXR signaling pathway (activated in both species) suggests an increase in lipogenesis, cholesterol efflux, and transport. This finding agrees with several studies that identified a dysregulation of the lipid transport system as a key signature of COVID-19 [69, 79]. And contrary to what we observed here, inhibition of the LXR/RXR pathway was associated with prolonged viral RNA shedding during COVID-19, often associated with carriers with increased contagion risk such as the elderly. A potential explanation is that we might not have captured this effect since we only studied lung tissues from acute SARS-CoV-2 infection in NHPs. Complete pathway results for olive baboons can be found in Suppl. Table S2.

Clinical relevance and study limitations

Acute respiratory distress in rhesus macaques and olive baboons partially recapitulates the progression of SARS-CoV-2 infection in humans, making them suitable animal models to test vaccines and therapies [9]. Indeed, our published studies of SARS-CoV-2 infection in NHP models indicate that both young and old rhesus macaques develop clinical signs of viral infection, mild-to-moderate pneumonitis, and

extra-pulmonary pathologies [9]. However, independent of their age, rhesus macaques can clear SARS-CoV-2 viral particles to undetectable levels within two weeks. Conversely, baboons have prolonged viral RNA shedding and substantially more lung inflammation compared with macaques, with higher lung inflammation in aged *vs.* young baboons [9].

Human proteomic studies provide a platform to uncover new molecular pathways associated with COVID-19 severity, identifying the involvement of complement factors, the coagulation system, inflammation modulators, and pro-inflammatory factors upstream and downstream of IL-6 [80, 81]. Indeed, a proteomics study identified inflammatory response modulator S100A8/A9 as being highly expressed in fatal COVID-19 cases [82]. Another study reported blood clot formation, severe extracellular matrix restructuring, and impaired tissue repair signaling in end-stage COVID-19 lung biopsies [6]. Other groups performed multiorgan proteomics analyses and revealed shared (e.g. RIPK1 or BRD4, the latter also showing altered expression in this study) and tissue-specific factors associated with SARS-CoV-2 infection, suggesting the need of organ-specific therapeutic interventions [83, 84]. However, most of these studies are performed in blood or serum (systemic changes) or are limited to post-mortem lung samples (tissue-specific responses), which are not easily available, with very few addressing COVID-19 lung-specific responses in aging individuals. NHP models that recapitulate COVID-19 pathology and progression represent a suitable alternative to address this gap in knowledge. Indeed, a COVID-19 infection model in cynomolgus macaques was able to recapitulate moderate COVID-19 symptoms [85].

In our current study we determined tissue-specific responses to SARS-CoV-2 infection using lung tissues from both young and aged NHPs (Fig. 3). Aged infected NHPs had significantly increased DAPs associated with regulation of the cytokine storm and the complement system (e.g. SAP, IGHM, JCHAIN, Clusterin). We also found increased DAPs associated with regulation of heart functions and the cardiovascular system (e.g. DSP, JUP, TPM4), specifically controlling blood flux. Indeed, aging plasma in healthy individuals was found enriched for heart and aorta specific proteins, revealing age-specific changes, which could potentially contribute to COVID-19 responses [86]. Other studies demonstrated that aged vascular endothelial cells (ECs) are highly susceptible to SARS-CoV-2 infection and subsequent endothelial dysfunction, resulting in fatal pneumonia with thrombosis in aged mice, suggesting age-associated EC responses in severe human COVID-19 [87, 88]. In this regard, L-arginine has been shown to enhance cardiac rehabilitation after myocardial infarction, whose risk is increased after COVID-19 [89, 90]. Proteins involved in clearance of cellular debris and

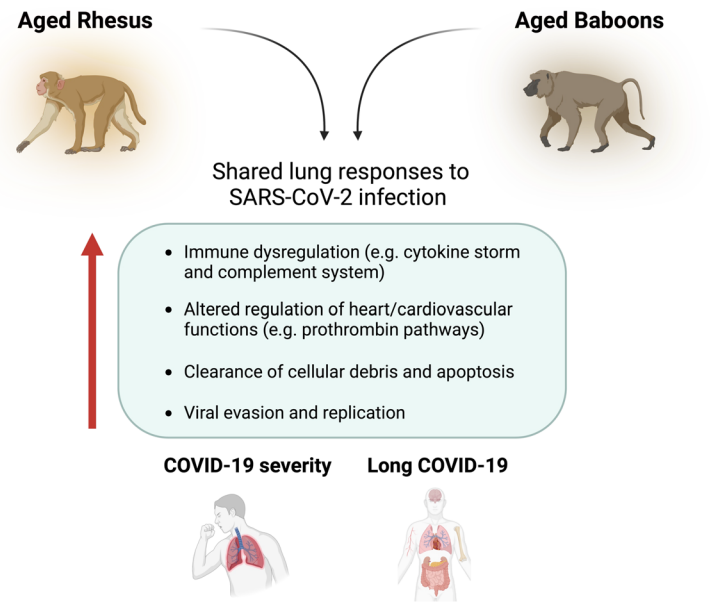

Fig. 3 Summary figure of shared lung responses to SARS-CoV-2 infection in aged rhesus macaques and olive baboons. Figure created with BioRender.com

apoptosis (e.g. Clusterin) were also more abundant in aged infected NHPs, as well as proteins involved in accelerating viral evasion and replication in host cells (e.g. RALY, RO60).

Proteins and pathways previously seen to be involved in long COVID (e.g. Pentraxin, IGHA, VEGF signaling) were also enriched in aged NHPs (Fig. 3). These findings suggest that aged NHPs can serve as a good model to study long-term health consequences and outcomes for long COVID-19, a poorly understood condition, especially in the elderly population [62]. Indeed, in the elderly, long COVID-19 seems to make existing chronic diseases worse, where elders with disorders such as heart failure, lung disease, or dementia, among others, develop more serious symptoms after recovering from COVID-19 [62].

Our results in the current study were limited by the number of available NHP lung tissue samples, which might not be representative of the overall NHP responses. In addition, samples from uninfected controls were not available, thus limiting our interpretation of the effect of SARS-CoV-2 infection (compared to uninfected NHPs), as well as the differences between young and aged NHPs at the baseline level (no infection). Indeed, lower pre-infection levels of HDL-cholesterol and vitamin D deficiency was associated with greater risk of adverse COVID-19 outcomes in elderly people [70, 91], as well as antecedent use of RASIs (renin–angiotensin system inhibitors) was associated with lower all-cause mortality in elderly hypertensive COVID-19 patients [92], which we were not able to determine here since pre-infection samples were not available. Further, the study had a single observation, at 14 days post-infection (necropsy timepoint), which did not allow us to study the proteome dynamics as disease progresses. Also, we used pre-existing tissue biopsies, previously snap-frozen, of approximately 0.5 cm^3. The small size of these biopsies meant we may not have captured all local responses to infection. Indeed, a deep spatial proteomics study of human lung autopsy specimens confirmed region-specific dysregulation of protein expression in key pulmonary structures, including alveolar epithelia, bronchial epithelia, and blood vessels, among others [7].

Despite these limitations, important findings were uncovered that support the use of these models as discovery agents for respiratory infectious diseases, especially in the context of aging where limited human samples are available. This and future studies can provide clues to delineate the mechanisms that explain why COVID-19 severity is increased in the elderly.

Acknowledgements We would like to thank Dr. Luis D. Giavedoni and the Southwest National Primate Research Center (SNPRC) Biorepository services for providing the NHP samples studied. We thank Dr. Luis Martinez-Sobrido and his laboratory personnel for providing the SARS-CoV-2 viral stock used in the original study to infect the NHP from which the samples were obtained. MS analyses were conducted in the Institutional Mass Spectrometry Laboratory of UT Health San Antonio, with support from UT Health San Antonio for the laboratory and the University of Texas System for purchase of the Orbitrap Fusion Lumos mass spectrometer. We thank Mr. Pardo and Ms. Molleur for their MS technical support.

Author contributions A.G.-V., A.A.-G. and A.A., sample processing and data analysis. S.T.W., DIA-MS analysis. D.K.S. provided samples. A.G.-V., J.B.T. study conceptualization, experimental design. A.G.-V., A.A.-G., N.M.C, and J.B.T wrote the manuscript. B.I.R., L.S.S., J.T., and J.B.T. provided funding and critical comments. All authors read and approved the final version of this manuscript.

Funding Studies supported by the National Institutes of Health/National Institute on Aging (NIH/NIA) 3P01-AG-051428-05S1 (Supplement) award to B.I.R., L.S.S., J.B.T. and J.T. A.G.-V., A.A.-G., and J.B.T. are part of the Interdisciplinary NextGen Tuberculosis Research Advancement Center (IN-TRAC) at Texas Biomed, which is supported by the NIH/National Institute of Allergy and Infectious Diseases (NIAID) under the award number P30-AI-168439. The content in this publication is solely the responsibility of the authors and does not necessarily represent the official views of the NIH.

Data availability Data supporting findings are available in Supplementary Materials. Raw Mass Spectrometry files and the Data-Independent Acquisition file are publicly available at MassIVE (ProteomeXchange consortium), http://massive.ucsd.edu, under MassIVE identifier: MSV000094333; ProteomeXchange identifier: PXD050683 (for both rhesus macaque and olive baboon species).

Declarations

Conflict of interest The authors declare no conflict of interest exists.

References

1. WHO (WHO). "WHO Coronavirus (COVID-19) Dashboard - https://covid19.who.int/." WHO. (accessed 2023).

2. Chen Y, et al. Aging in COVID-19: Vulnerability, immunity and intervention. Ageing Res Rev. 2021;65:101205. https://doi.org/10.1016/j.arr.2020.101205.
3. O'Driscoll M, et al. Age-specific mortality and immunity patterns of SARS-CoV-2. Nature. 2021;590(7844):140–5. https://doi.org/10.1038/s41586-020-2918-0.
4. Farshbafnadi M, Kamali Zonouzi S, Sabahi M, Dolatshahi M, Aarabi MH. Aging & COVID-19 susceptibility, disease severity, and clinical outcomes: The role of entangled risk factors. Exp Gerontol. 2021;154:111507. https://doi.org/10.1016/j.exger.2021.111507.
5. Yanez ND, Weiss NS, Romand JA, Treggiari MM. COVID-19 mortality risk for older men and women. BMC Public Health. 2020;20(1):1742. https://doi.org/10.1186/s12889-020-09826-8.
6. Gindlhuber J, et al. Proteomic profiling of end-stage COVID-19 lung biopsies. Clin Proteomics. 2022;19(1):46. https://doi.org/10.1186/s12014-022-09386-6.
7. Mao Y, et al. Deep spatial proteomics reveals region-specific features of severe COVID-19-related pulmonary injury. Cell Rep. 2024;43(2):113689. https://doi.org/10.1016/j.celrep.2024.113689.
8. Nie X, et al. Multi-organ proteomic landscape of COVID-19 autopsies. Cell. 2021;184(3):775-791.e14. https://doi.org/10.1016/j.cell.2021.01.004.
9. Singh DK, et al. Responses to acute infection with SARS-CoV-2 in the lungs of rhesus macaques, baboons and marmosets. Nat Microbiol. 2021;6(1):73–86. https://doi.org/10.1038/s41564-020-00841-4.
10. Trichel AM. Overview of Nonhuman Primate Models of SARS-CoV-2 Infection. Comp Med. 2021;71(5):411–32. https://doi.org/10.30802/AALAS-CM-20-000119.
11. Singh DK, et al. Myeloid cell interferon responses correlate with clearance of SARS-CoV-2. Nat Commun. 2022;13(1):679. https://doi.org/10.1038/s41467-022-28315-7.
12. Rosa BA, et al. IFN signaling and neutrophil degranulation transcriptional signatures are induced during SARS-CoV-2 infection. Commun Biol. 2021;4(1):290. https://doi.org/10.1038/s42003-021-01829-4.
13. Searle BC, et al. Chromatogram libraries improve peptide detection and quantification by data independent acquisition mass spectrometry. Nat Commun. 2018;9(1):5128. https://doi.org/10.1038/s41467-018-07454-w.
14. Gessulat S, et al. Prosit: proteome-wide prediction of peptide tandem mass spectra by deep learning. Nat Methods. 2019;16(6):509–18. https://doi.org/10.1038/s41592-019-0426-7.
15. Broom BM, et al. A Galaxy Implementation of Next-Generation Clustered Heatmaps for Interactive Exploration of Molecular Profiling Data. Cancer Res. 2017;77(21):e23–6. https://doi.org/10.1158/0008-5472.CAN-17-0318.
16. M. C. Ryan et al. "Interactive clustered heat map builder: An easy web-based tool for creating sophisticated clustered heat maps." F1000Res, 2019;8. https://doi.org/10.12688/f1000research.20590.2.
17. Zinellu A, Paliogiannis P, Carru C, Mangoni AA. Serum amyloid A concentrations, COVID-19 severity and mortality: An updated systematic review and meta-analysis. Int J Infect Dis. 2021;105:668–74. https://doi.org/10.1016/j.ijid.2021.03.025.
18. Almusalami EM, Lockett A, Ferro A, Posner J. Serum amyloid A-A potential therapeutic target for hyper-inflammatory syndrome associated with COVID-19. Front Med (Lausanne). 2023;10:1135695. https://doi.org/10.3389/fmed.2023.1135695.
19. V. Gallo ,et al. "Clinical, immunological, and functional characterization of six patients with very high IgM levels." J Clin Med, 2020;9(3). https://doi.org/10.3390/jcm9030818.
20. Sobhy H. The potential functions of protein domains during COVID infection: An analysis and a review. COVID Rev. 2021;1:384–93. https://doi.org/10.3390/covid1010032.
21. Serra-Pages C, Medley QG, Tang M, Hart A, Streuli M. Liprins, a family of LAR transmembrane protein-tyrosine phosphatase-interacting proteins. J Biol Chem. 1998;273(25):15611–20. https://doi.org/10.1074/jbc.273.25.15611.
22. Christie JD, et al. Genome wide association identifies PPFIA1 as a candidate gene for acute lung injury risk following major trauma. PLoS One. 2012;7(1): e28268. https://doi.org/10.1371/journal.pone.0028268.
23. Rodwell GE, et al. A transcriptional profile of aging in the human kidney. PLoS Biol. 2004;2(12):e427. https://doi.org/10.1371/journal.pbio.0020427.
24. K. B. Karunakaran, N. Balakrishnan, M. K. Ganapathiraju. "Interactome of SARS-CoV-2 / nCoV19 modulated host proteins with computationally predicted PPIs." Res Sq, 2020. https://doi.org/10.21203/rs.3.rs-28592/v1.
25. Labeau A, et al. Characterization and functional interrogation of the SARS-CoV-2 RNA interactome. Cell Rep. 2022;39(4):110744. https://doi.org/10.1016/j.celrep.2022.110744.
26. Walker AP, Fodor E. Interplay between Influenza Virus and the Host RNA Polymerase II Transcriptional Machinery. Trends Microbiol. 2019;27(5):398–407. https://doi.org/10.1016/j.tim.2018.12.013.
27. Diamant G, Bahat A, Dikstein R. The elongation factor Spt5 facilitates transcription initiation for rapid induction of inflammatory-response genes. Nat Commun. 2016;7:11547. https://doi.org/10.1038/ncomms11547.
28. A. Lal, M. Galvao Ferrarini, A. J. Gruber, "Investigating the Human Host-ssRNA Virus Interaction Landscape Using the SMEAGOL Toolbox." Viruses, 2022;14(7). https://doi.org/10.3390/v14071436.
29. Fujii H, et al. High levels of anti-SSA/Ro antibodies in COVID-19 patients with severe respiratory failure: a case-based review : High levels of anti-SSA/Ro antibodies in COVID-19. Clin Rheumatol. 2020;39(11):3171–5. https://doi.org/10.1007/s10067-020-05359-y.
30. Zhang Q, et al. Nuclear speckle specific hnRNP D-like prevents age- and AD-related cognitive decline by modulating RNA splicing. Mol Neurodegener. 2021;16(1):66. https://doi.org/10.1186/s13024-021-00485-w.
31. Wang C, et al. Abnormal global alternative RNA splicing in COVID-19 patients. PLoS Genet. 2022;18(4):e1010137. https://doi.org/10.1371/journal.pgen.1010137.
32. Johansen MD, et al. Increased SARS-CoV-2 Infection, Protease, and Inflammatory Responses in Chronic Obstructive Pulmonary Disease Primary Bronchial

Epithelial Cells Defined with Single-Cell RNA Sequencing. Am J Respir Crit Care Med. 2022;206(6):712–29. https://doi.org/10.1164/rccm.202108-1901OC.
33. van Moorsel CHM. Desmoplakin: An Important Player in Aging Lung Disease. Am J Respir Crit Care Med. 2020;202(9):1201–2. https://doi.org/10.1164/rccm.202006-2457ED.
34. Rezaei Bookani K, et al. A case series of desmoplakin cardiomyopathy: a mimic of viral myocarditis. Eur Heart J Case Rep. 2022;6(8):ytac341. https://doi.org/10.1093/ehjcr/ytac341.
35. Chen Y, et al. 2022 "Immune response pattern across the asymptomatic, symptomatic and convalescent periods of COVID-19,." Biochim Biophys Acta Proteins Proteom. 1870;2:140736. https://doi.org/10.1016/j.bbapap.2021.140736.
36. Wang JY, Zhang W, Roehrl MW, Roehrl VB, Roehrl MH. An autoantigen profile of human A549 lung cells reveals viral and host etiologic molecular attributes of autoimmunity in COVID-19. J Autoimmun. 2021;120:102644. https://doi.org/10.1016/j.jaut.2021.102644.
37. Neikirk K, et al. Latent transforming growth factor beta binding protein 4: A regulator of mitochondrial function in acute kidney injury. Aging Cell. 2023;22(12):e14019. https://doi.org/10.1111/acel.14019.
38. M. Fassan, et al. "Multi-design differential expression profiling of COVID-19 lung autopsy specimens reveals significantly deregulated inflammatory pathways and SFTPC impaired transcription." Cells, 2022;11(6). https://doi.org/10.3390/cells11061011.
39. Debaize L, Troadec MB. The master regulator FUBP1: its emerging role in normal cell function and malignant development. Cell Mol Life Sci. 2019;76(2):259–81. https://doi.org/10.1007/s00018-018-2933-6.
40. Shi W, et al. Integration of risk variants from GWAS with SARS-CoV-2 RNA interactome prioritizes FUBP1 and RAB2A as risk genes for COVID-19. Sci Rep. 2023;13(1):19194. https://doi.org/10.1038/s41598-023-44705-3.
41. Y. Zhou, et al. "A comprehensive SARS-CoV-2-human protein-protein interactome network identifies pathobiology and host-targeting therapies for COVID-19." Res Sq, 2022. https://doi.org/10.21203/rs.3.rs-1354127/v2.
42. J. Sun, Y. Gui, S. Zhou, X. L. Zheng. "Unlocking the secrets of aging: Epigenetic reader BRD4 as the target to combatting aging-related diseases." J Adv Res, 2023. https://doi.org/10.1016/j.jare.2023.11.006.
43. Mills RJ, et al. BET inhibition blocks inflammation-induced cardiac dysfunction and SARS-CoV-2 infection. Cell. 2021;184(8):2167-2182.e22. https://doi.org/10.1016/j.cell.2021.03.026.
44. Nixon RA. The calpains in aging and aging-related diseases. Ageing Res Rev. 2003;2(4):407–18. https://doi.org/10.1016/s1568-1637(03)00029-1.
45. Kovacs L, Su Y. Redox-dependent Calpain signaling in airway and pulmonary vascular remodeling in COPD. Adv Exp Med Biol. 2017;967:139–60. https://doi.org/10.1007/978-3-319-63245-2_9.
46. Juibari AD, Rezadoost MH, Soleimani M. The key role of Calpain in COVID-19 as a therapeutic strategy. Inflammopharmacology. 2022;30(5):1479–91. https://doi.org/10.1007/s10787-022-01002-1.
47. Inal J, Paizuldaeva A, Terziu E. Therapeutic use of calpeptin in COVID-19 infection. Clin Sci (Lond). 2022;136(20):1439–47. https://doi.org/10.1042/CS20220638.
48. Ma C, et al. Boceprevir, GC-376, and calpain inhibitors II, XII inhibit SARS-CoV-2 viral replication by targeting the viral main protease. Cell Res. 2020;30(8):678–92. https://doi.org/10.1038/s41422-020-0356-z.
49. H. Li, et al. "The structure, function and regulation of protein tyrosine phosphatase receptor type J and its role in diseases." Cells, 2022;12(1). https://doi.org/10.3390/cells12010008.
50. Rodriguez-Galan I, Albaladejo-Blazquez N, Ruiz-Robledillo N, Pascual-Lledo JF, Ferrer-Cascales R, Gil-Carbonell J. Impact of COVID-19 on quality of life in survivors with pulmonary sequelae. Sci Rep. 2024;14(1):6926. https://doi.org/10.1038/s41598-024-57603-z.
51. Chen Z, et al. Interactomes of SARS-CoV-2 and human coronaviruses reveal host factors potentially affecting pathogenesis. Embo J. 2021;40(17):e107776. https://doi.org/10.15252/embj.2021107776.
52. Crupi L, Capra AP, Pantò G, Repici A, Calapai F, Squeri R, Ardizzone A, Esposito E. Serum Pentraxin 3 as promising biomarker for the long-lasting inflammatory response of COVID-19. Int J Mol Sci. 2023;24(18):14195. https://doi.org/10.3390/ijms241814195.
53. Graham LC, et al. Regional molecular mapping of primate synapses during normal healthy aging. Cell Rep. 2019;27(4):1018-1026.e4. https://doi.org/10.1016/j.celrep.2019.03.096.
54. G. C. Lechuga, et al. "SARS-CoV-2 Proteins Bind to Hemoglobin and Its Metabolites." Int J Mol Sci, 2021;22(16). https://doi.org/10.3390/ijms22169035.
55. Batory G, Jancso A, Puskas E, Redei A, Lengyel E. Antibody and immunoglobulin levels in aged humans. Arch Gerontol Geriatr. 1984;3(2):175–88. https://doi.org/10.1016/0167-4943(84)90009-8.
56. D. Sterlin, et al. "IgA dominates the early neutralizing antibody response to SARS-CoV-2." Sci Transl Med 2021;13(577). https://doi.org/10.1126/scitranslmed.abd2223.
57. Farooq H, Ur Rehman MA, Asmar A, Asif S, Mushtaq A, Qureshi MA. The pathogenesis of COVID-19-induced IgA nephropathy and IgA vasculitis: A systematic review. J Taibah Univ Med Sci. 2022;17(1):1–13. https://doi.org/10.1016/j.jtumed.2021.08.012.
58. George PM, et al. A persistent neutrophil-associated immune signature characterizes post-COVID-19 pulmonary sequelae. Sci Transl Med. 2022;14(671):eabo5795. https://doi.org/10.1126/scitranslmed.abo5795.
59. D. Bojkova, et al. "Targeting the pentose phosphate pathway for SARS-CoV-2 therapy." Metabolites,2021;11(10). https://doi.org/10.3390/metabo11100699.
60. Varela AA, Cheng S, Werren JH. Novel ACE2 protein interactions relevant to COVID-19 predicted by evolutionary rate correlations. PeerJ. 2021;9:e12159. https://doi.org/10.7717/peerj.12159.

61. Habiel DM, et al. Divergent roles for clusterin in lung injury and repair. Sci Rep. 2017;7(1):15444. https://doi.org/10.1038/s41598-017-15670-5.
62. Mansell V, Hall Dykgraaf S, Kidd M, Goodyear-Smith F. Long COVID and older people. Lancet Healthy Longev. 2022;3(12):e849–54. https://doi.org/10.1016/S2666-7568(22)00245-8.
63. R. Talotta. "Impaired VEGF-A-Mediated neurovascular crosstalk induced by SARS-CoV-2 spike protein: A potential hypothesis explaining long COVID-19 symptoms and COVID-19 vaccine side effects?." Microorganisms, 2022;10(12). https://doi.org/10.3390/microorganisms10122452.
64. M. Aminpour, S. Hameroff, J. A. Tuszynski, "How COVID-19 hijacks the cytoskeleton: therapeutic implications." Life (Basel), 2022; 12(6). https://doi.org/10.3390/life12060814.
65. Liu J, Lu F, Chen Y, Plow E, Qin J. Integrin mediates cell entry of the SARS-CoV-2 virus independent of cellular receptor ACE2. J Biol Chem. 2022;298(3):101710. https://doi.org/10.1016/j.jbc.2022.101710.
66. Mezu-Ndubuisi OJ, Maheshwari A. The role of integrins in inflammation and angiogenesis. Pediatr Res. 2021;89(7):1619–26. https://doi.org/10.1038/s41390-020-01177-9.
67. D. L. Ng et al. "A diagnostic host response biosignature for COVID-19 from RNA profiling of nasal swabs and blood." Sci Adv, 2021; 7(6). https://doi.org/10.1126/sciadv.abe5984.
68. De R, Azad RK. Molecular signatures in the progression of COVID-19 severity. Sci Rep. 2022;12(1):22058. https://doi.org/10.1038/s41598-022-26657-2.
69. Lipman D, Safo SE, Chekouo T. Multi-omic analysis reveals enriched pathways associated with COVID-19 and COVID-19 severity. PLoS One. 2022;17(4):e0267047. https://doi.org/10.1371/journal.pone.0267047.
70. Mostaza JM, et al. Pre-infection HDL-cholesterol levels and mortality among elderly patients infected with SARS-CoV-2. Atherosclerosis. 2022;341:13–9. https://doi.org/10.1016/j.atherosclerosis.2021.12.009.
71. Li Q, Chen Z, Zhou X, Li G, Zhang C, Yang Y. Ferroptosis and multi-organ complications in COVID-19: mechanisms and potential therapies. Front Genet. 2023;14:1187985. https://doi.org/10.3389/fgene.2023.1187985.
72. Singh DG, Singh SR, Cole B, Alfson J, Clemmons KJ, Gazi E, Gonzalez M, Escobedo O, Lee R, Chatterjee T-H, Goez-Gazi A, Sharan Y, Thippeshappa R, Gough R, Alvarez M, Blakley C, Ferdin A, Bartley J, Staples C, Parodi H, Callery P, Mannino J, Klaffke A, Escareno B, PlattII P, Hodara RN, Scordo V, Oyejide JM, Ajithdoss A, Copin DK, Baum R, Kyratsous A, Alvarez C, Rosas X, Ahmed B, Goodroe M, Dutton A, Hall-Ursone J, Frost S, Voges PA, Ross AK, Sayers CN, Chen K, Hallam C, Khader C, Mitreva SA, Anderson M, Martinez-Sobrido TJC, Patterson L, Turner JL, Torrelles J, Dick JB Jr, Brasky EJ, Schlesinger K, Giavedoni LS, Carrion LD Jr, Kaushal RD. Responses to acute infection with SARS-CoV-2 in the lungs of rhesus macaques, baboons and marmosets. Nat Microbiol. 2020;6(1):73–86.
73. A. Garcia-Vilanova, et al. "The aging human lung mucosa: A proteomics study." J Gerontol: Series A, 2022;091. https://doi.org/10.1093/gerona/glac091
74. Yu J, et al. Complement dysregulation is associated with severe COVID-19 illness. Haematologica. 2022;107(5):1095–105. https://doi.org/10.3324/haematol.2021.279155.
75. Sayit AT, Elmali M, Deveci A, Gedikli O. Relationship between acute phase reactants and prognosis in patients with or without COVID-19 pneumonia. Rev Inst Med Trop Sao Paulo. 2021;63:e51. https://doi.org/10.1590/S1678-9946202163051.
76. Demichev V, et al. A time-resolved proteomic and prognostic map of COVID-19. Cell Syst. 2021;12(8):780-794.e7. https://doi.org/10.1016/j.cels.2021.05.005.
77. Yuan X, Tong X, Wang Y, Wang H, Wang L, Xu X. Coagulopathy in elderly patients with coronavirus disease 2019. Aging Med (Milton). 2020;3(4):260–5. https://doi.org/10.1002/agm2.12133.
78. Skendros P, et al. Complement C3 inhibition in severe COVID-19 using compstatin AMY-101. Sci Adv. 2022;8(33):eabo2341. https://doi.org/10.1126/sciadv.abo2341.
79. Overmyer KA, et al. Large-Scale Multi-omic Analysis of COVID-19 Severity. Cell Syst. 2021;12(1):23-40.e7. https://doi.org/10.1016/j.cels.2020.10.003.
80. Messner CB, et al. Ultra-High-Throughput Clinical Proteomics Reveals Classifiers of COVID-19 Infection. Cell Syst. 2020;11(1):11-24.e4. https://doi.org/10.1016/j.cels.2020.05.012.
81. Yin S, et al. Integrated Immunopeptidomic and Proteomic Analysis of COVID-19 lung biopsies. Front Immunol. 2023;14:1269335. https://doi.org/10.3389/fimmu.2023.1269335.
82. Wu M, et al. Transcriptional and proteomic insights into the host response in fatal COVID-19 cases. Proc Natl Acad Sci U S A. 2020;117(45):28336–43. https://doi.org/10.1073/pnas.2018030117.
83. Feng L, et al. Proteome-wide data analysis reveals tissue-specific network associated with SARS-CoV-2 infection. J Mol Cell Biol. 2020;12(12):946–57. https://doi.org/10.1093/jmcb/mjaa033.
84. Schweizer L, et al. Quantitative multiorgan proteomics of fatal COVID-19 uncovers tissue-specific effects beyond inflammation. EMBO Mol Med. 2023;15(9):e17459. https://doi.org/10.15252/emmm.202317459.
85. Wang T, et al. Proteomic and metabolomic characterization of SARS-CoV-2-Infected cynomolgus macaque at early stage. Front Immunol. 2022;13:954121. https://doi.org/10.3389/fimmu.2022.954121.
86. Arthur L, et al. Cellular and plasma proteomic determinants of COVID-19 and non-COVID-19 pulmonary diseases relative to healthy aging. Nat Aging. 2021;1(6):535–49. https://doi.org/10.1038/s43587-021-00067-x.
87. Urata R, et al. Senescent endothelial cells are predisposed to SARS-CoV-2 infection and subsequent endothelial dysfunction. Sci Rep. 2022;12(1):11855. https://doi.org/10.1038/s41598-022-15976-z.
88. Tsumita T, et al. Viral uptake and pathophysiology of the lung endothelial cells in age-associated

severe SARS-CoV-2 infection models. Aging Cell. 2024;23(2):e14050. https://doi.org/10.1111/acel.14050.
89. Mone P, et al. L-Arginine enhances the effects of cardiac rehabilitation on physical performance: New insights for managing cardiovascular patients during the COVID-19 pandemic. J Pharmacol Exp Ther. 2022;381(3):197–203. https://doi.org/10.1124/jpet.122.001149.
90. Zuin M, Rigatelli G, Battisti V, Costola G, Roncon L, Bilato C. Increased risk of acute myocardial infarction after COVID-19 recovery: A systematic review and meta-analysis. Int J Cardiol. 2023;372:138–43. https://doi.org/10.1016/j.ijcard.2022.12.032.
91. M. Drame, et al. "Relation between Vitamin D and COVID-19 in Aged People: A systematic review." Nutrients, 2021;13(4). https://doi.org/10.3390/nu13041339.
92. Gori M, et al. Association between inhibitors of the renin-angiotensin system and lung function in elderly patients recovered from severe COVID-19. Eur J Prev Cardiol. 2022;29(5):e196–9. https://doi.org/10.1093/eurjpc/zwab143.